Truncation and Indirect Incremental Methods in Hencky's Perfect Plasticity

Stanislav Sysala and Jaroslav Haslinger

Abstract The contribution is concerned with reliable and computable bounds of the limit (or safety) load in the deformation theory of perfect plasticity. We consider truncation and indirect incremental methods of limit analysis which can be interpreted as penalization techniques. Further, convergence for higher order finite elements is shown. The efficiency of the proposed approaches is illustrated on numerical experiments with the von Mises and Drucker–Prager yield criteria.

1 Introduction

The paper is focused on reliable and easily computable bounds of limit loads in elastic-perfectly plastic problems. We summarize and slightly extend the results presented in [2, 7, 8, 12]. In particular, we extend the finite element analysis to higher order elements to reduce the observed locking effect.

The paper is organized as follows. Section 2 contains preliminaries from the generalized Hencky plasticity and the related limit analysis. The von Mises and Drucker–Prager yield criteria are mentioned as particular cases. Section 3 is devoted to the truncation method where unbounded yield surfaces are approximated by bounded ones. The indirect incremental method is introduced in Sect. 4. Both methods are firstly defined for the continuous setting of the problem in order to demonstrate their independency of the problem discretization. The discretized problem is analyzed in Sect. 5. Section 6 summarizes our strategy how to find computable and reliable lower and upper bounds of λ^*. The lower and upper bounds of the limit load λ^* for two model examples with the above mentioned yield criteria are established. Unlike [8], we consider P_2-elements and different meshes, geometries or elastic parameters in order to improve the bounds.

S. Sysala (✉) J. Haslinger
Institute of Geonics of the Czech Academy of Sciences, Ostrava, Czech Republic
e-mail: stanislav.sysala@ugn.cas.cz

J. Haslinger
Charles University, Prague, Czech Republic
e-mail: hasling@karlin.mff.cuni.cz

F. dell'Isola et al. (eds.), *Mathematical Modelling in Solid Mechanics*,
Advanced Structured Materials 69, DOI 10.1007/978-981-10-3764-1_17

2 Generalized Hencky Plasticity Problem

2.1 Basic Definitions and Properties

The classical Hencky plasticity model of the deformation plasticity theory is based on the von Mises yield law. Since an abstract yield criterion is used we rather write "generalized" Hencky plasticity model in order to stress this fact. This static model is usually completed by a parametric study in order to be close to the incremental (quasistatic) theory of elasto-plasticity. The parametrized model is sufficient to treat the limit load analysis. For more details, we refer to, e.g., [6, 7, 14].

The space of admissible displacement fields has the form

$$\mathbb{V} = \{v \in H^1(\Omega; \mathbb{R}^3) \mid v|_{\Gamma_D} = 0\},$$

where Ω is a *bounded* domain with the Lipschitz continuous boundary $\partial\Omega$ and Γ_D, Γ_N are open and nonempty parts of $\partial\Omega$ such that $\Gamma_D \cap \Gamma_N = \emptyset$ and $\bar{\Gamma}_D \cup \bar{\Gamma}_N = \partial\Omega$. Further, $f \in L^2(\Gamma_N; \mathbb{R}^3)$, $F \in L^2(\Omega; \mathbb{R}^3)$ denote the density of surface and volume forces, respectively, and

$$L(v) = \int_\Omega F \cdot v \, dx + \int_{\Gamma_N} f \cdot v \, ds, \quad v \in \mathbb{V}, \qquad \|F\|_{L^2(\Omega;\mathbb{R}^3)} + \|f\|_{L^2(\Gamma_N;\mathbb{R}^3)} \neq 0. \tag{1}$$

Stress and strain tensors are represented locally by symmetric matrices, i.e., elements of $\mathbb{R}^{3\times3}_{sym}$. In particular, we consider the infinitesimal small strain tensor represented by a symmetric part of the displacement gradient:

$$\varepsilon(v) = \frac{1}{2}(\nabla v + (\nabla v)^T).$$

The biscalar product and the corresponding norm in $\mathbb{R}^{3\times3}_{sym}$ will be denoted by $e : \eta = e_{ij}\eta_{ij}$ and $\|e\|^2 = e : e$ for any $e, \eta \in \mathbb{R}^{3\times3}_{sym}$, respectively.

Let B be a closed, convex subset of $\mathbb{R}^{3\times3}_{sym}$ containing a vicinity of the origin. This set represents *plastically admissible stresses* and it is defined by a plastic criterion, see Sects. 2.2 or 2.3. To formulate the constitutive stress-strain relation we introduce the function Π_B which is a *generalized* projection of $\mathbb{R}^{3\times3}_{sym}$ onto B (in the sense of [11]):

$$\Pi_B : e \mapsto \Pi_B(e), \quad \|\mathbb{C}e - \Pi_B(e)\|_{\mathbb{C}^{-1}} = \min_{\tau\in B} \|\mathbb{C}e - \tau\|_{\mathbb{C}^{-1}}, \quad e \in \mathbb{R}^{3\times3}_{sym},$$

where $\mathbb{C} : \mathbb{R}^{3\times3}_{sym} \to \mathbb{R}^{3\times3}_{sym}$ is a linear, positive definite, fourth order elasticity tensor characterizing the elastic material response, $\mathbb{C}^{-1}$ is the corresponding inverse and $\|\tau\|^2_{\mathbb{C}^{-1}} := \mathbb{C}^{-1}\tau : \tau$ for any $\tau \in \mathbb{R}^{3\times3}_{sym}$. The potential $j : \mathbb{R}^{3\times3}_{sym} \to \mathbb{R}_+$ of Π_B is defined by

$$j(e) = \sup_{\tau \in B} \left\{ \tau : e - \frac{1}{2} \|\tau\|^2_{\mathbb{C}^{-1}} \right\}, \quad e \in \mathbb{R}^{3\times 3}_{sym}. \tag{2}$$

It is a convex, continuously Fréchet differentiable function, and

$$\frac{\varepsilon}{2}\|e\|_{\mathbb{C}} - \frac{\varepsilon^2}{8} \le j(e) \le \frac{1}{2}\|e\|^2_{\mathbb{C}}, \quad \|e\|^2_{\mathbb{C}} := \mathbb{C}e : e, \quad \forall e \in \mathbb{R}^{3\times 3}_{sym}, \tag{3}$$

where $\varepsilon > 0$ is such that the ball $\{\tau \in \mathbb{R}^{3\times 3}_{sym} \mid \|\tau\|_{\mathbb{C}^{-1}} \le \varepsilon\}$ belongs to B. Thus, only a linear growth of j at infinity is guaranteed.

The generalized Hencky plasticity problem (in terms of displacements) for a given value of the load parameter $\lambda \ge 0$ reads as follows:

$$(\mathscr{P})_\lambda \qquad \inf_{v \in V} J_\lambda(v), \quad J_\lambda(v) = \int_\Omega j(\varepsilon(v))\, dx - \lambda L(v).$$

Notice that J_λ need not be bounded from below for all $\lambda > 0$ due to the lower bound of j in (3). Moreover, even if J_λ is bounded from below, problem $(\mathscr{P})_\lambda$ need not have a minimizer belonging to $\mathbb{V}$. For the existence analysis, it is necessary to use the relaxation of the problem including the extension of $\mathbb{V}$ to the BD-space of functions with bounded deformations, see, e.g., [10, 14]. This space allows discontinuities of displacements along surfaces in 3D and thus the model is capable to predict possible failure zones in the investigated body. This fact will be illustrated in Sect. 6.

In order to decide whether J_λ is bounded from below in $\mathbb{V}$ or not, it is natural to introduce the limit load parameter

$$\lambda^* = \sup \left\{ \lambda \ge 0 \mid \inf_{v \in \mathbb{V}} J_\lambda(v) > -\infty \right\}. \tag{4}$$

This definition also admits the value $\lambda^* = +\infty$, however λ^* is usually finite in meaningful settings of the problem. One can easily check that the function $\phi(\lambda) = \inf_{v\in\mathbb{V}} J_\lambda(v)$ is decreasing on $(0, \lambda^*)$ and thus J_λ is bounded from below for any $\lambda < \lambda^*$. Other straightforward but useful consequences of (4) are introduced in the following lemma.

Lemma 1 (Basic bounds of λ^*.)

(i) Let $j_1, j_2 : \mathbb{R}^{3\times 3}_{sym} \to \mathbb{R}_+ \cup \{+\infty\}$, $0 \le j_1 \le j_2$, be two convex and proper functions. Then the corresponding limit load parameters λ_1^*, λ_2^* defined by (4) satisfy $\lambda_1^* \le \lambda_2^*$.

(ii) Let K be a subset of $\mathbb{V}$ and $\lambda_K^* := \sup\{\lambda \ge 0 \mid \inf_{v\in K} J_\lambda(v) > -\infty\}$. Then $\lambda^* \le \lambda_K^*$.

For the limit analysis, it is very useful to introduce a special minimization problem. Following [8], we firstly consider the function

$$j_\alpha(e) = \frac{1}{\alpha} j(\alpha e) \quad \forall e \in \mathbb{R}^{3\times 3}_{sym}, \quad \alpha > 0. \tag{5}$$

As for j, one can define the corresponding limit parameter λ^*_α. By substitution, we have:

$$\inf_{v\in V}\left[\int_\Omega j_\alpha(\varepsilon(v))\,dx - \lambda L(v)\right] = \frac{1}{\alpha}\inf_{v\in V}\left[\int_\Omega j(\varepsilon(v))\,dx - \lambda L(v)\right] \quad \forall \alpha > 0.$$

Hence, $\lambda^*_\alpha = \lambda^*$ for any $\alpha > 0$. Next, define the function

$$\begin{aligned} &j_\infty : \mathbb{R}^{3\times 3}_{sym} \to \overline{\mathbb{R}}_+, \quad \overline{\mathbb{R}}_+ := \mathbb{R}_+ \cup \{+\infty\}, \\ &j_\infty(e) = \lim_{\alpha\to+\infty} j_\alpha(e) = \sup_{\tau\in B} \tau : e, \quad e \in \mathbb{R}^{3\times 3}_{sym}. \end{aligned} \tag{6}$$

Clearly, $j_\infty(0) = 0$ and j_∞ is a proper, convex function in $\mathbb{R}^{3\times 3}_{sym}$ which is also positively 1 - homogeneous. Further, it holds:

$$j \le j_\alpha \le j_\infty \quad \forall \alpha \ge 1. \tag{7}$$

The limit load parameter associated with j_∞ is defined as follows:

$$\zeta^* = \sup\left\{\lambda \ge 0 \mid \inf_{v\in\mathbb{V}}\left[\int_\Omega j_\infty(\varepsilon(v))\,dx - \lambda L(v)\right] > -\infty\right\}. \tag{8}$$

It is readily seen that

$$\lambda^* \le \zeta^*, \tag{9}$$

making use of (7) and Lemma 1, i.e., ζ^* is in an upper bound of the limit load parameter λ^*. The properties of j_∞ enable us to derive a more convenient definition of ζ^* than (8), see, e.g., [8].

Lemma 2 *It holds:*

$$\zeta^* = \inf_{\substack{v\in\mathbb{V}\\ L(v)=1}} J_\infty(v), \qquad J_\infty(v) = \int_\Omega j_\infty(\varepsilon(v))\,dx, \quad v \in \mathbb{V}. \tag{10}$$

Remark 1 The inf-problem (10) is termed the *problem of limit analysis* using the terminology of perfect plasticity [4, 14]. This minimization problem is important from several reasons:

- It enables us to estimate λ^* by a straightforward manner (minimization), see e.g., in [1, 4]. Moreover, the values $J_\infty(v)$, where $v \in \mathbb{V}$, $L(v) = 1$ and $v \in \operatorname{dom} J_\infty$, are the guaranteed upper bounds of λ^*.
- The inf-problem (10) is in a certain sense dual to the sup-problem (4) defining λ^*. Using the duality approach, one can prove that $\lambda^* = \zeta^*$ for some sets B.

- It is well-known that the additional constraint $v \in \mathrm{dom} J_\infty = \{w \in \mathbb{V} \mid J_\infty(w) < +\infty\}$ may cause locking effect in perfect plasticity. For example, if B represents the von Mises yield criterion then the divergence free constraint appears, see Sect. 2.2.
- The limit load parameters λ^* and ζ^* are independent of the elasticity tensor $\mathbb{C}$. For ζ^* this fact follows from the sup-definition of j_∞ in (6) and for λ^* from the duality approach. This simple observation is useful mainly for soil materials with the Poisson ratio close to the critical value 0.5 when significant rounding errors of numerical solutions arise.
- The formation of failure zones producing discontinuities of displacements is typical for the limit load. From (10), it seems to be natural that values of j_∞ vanish far from the expected failure during the minimization. On such subdomains, one can expect rigid body displacements. This will be illustrated on numerical examples in Sect. 6. In particular, in Sect. 6.3, we will study the slope stability benchmark where the failure is localized only in a vicinity of the slope. Moreover, the expected rigid body displacements far from the slope vanish due to prescribed boundary conditions. This leads to a simple observation that the limit parameter remains unchanged when we use a much smaller domain than in [5, 8, 13].

In the subsequent parts of this section, we introduce the von Mises and Drucker–Prager yield criteria as particular examples of B.

2.2 The Von Mises Yield Criterion

The set B defined by the von Mises yield criterion has the form

$$B = \left\{\tau \in \mathbb{R}^{3\times 3}_{sym} \mid \ \|\tau^D\| \le \gamma\right\}, \tag{11}$$

where $\|\tau^D\|^2 := \tau^D : \tau^D$, $\tau^D = \tau - \frac{1}{3}(tr\,\tau)\iota$ is the deviatoric part of τ, $tr\,\tau = \tau_{ii}$ is the trace of τ, $\iota = \mathrm{diag}(1, 1, 1)$ is the unit matrix, and $\gamma > 0$ represents an initial yield stress. Notice that B is the unbounded cylinder with the (hydrostatic) axis $\{\tau \in \mathbb{R}^{3\times 3}_{sym} \mid \tau = a\iota, \quad a \in \mathbb{R}\}$. If the elastic stress-strain relation is isotropic and expressed in terms of the bulk ($K > 0$) and shear ($G > 0$) moduli, i.e.,

$$\tau = \mathbb{C}e = K(tr\,e)\iota + 2Ge^D \quad \forall e \in \mathbb{R}^{3\times 3}_{sym}, \tag{12}$$

then j defined by (2) can be written as

$$j(e) = \begin{cases} \frac{1}{2}K(tr\,e)^2 + G\|e^D\|^2, & \text{if } 2G\|e^D\| \le \gamma \\ \frac{1}{2}K(tr\,e)^2 + \gamma\|e^D\| - \frac{\gamma^2}{4G}, & \text{if } 2G\|e^D\| > \gamma \end{cases}, \quad \forall e \in \mathbb{R}^{3\times 3}_{sym},$$

see, e.g., [14]. It is readily seen that

$$j_\infty(e) = \lim_{\alpha\to+\infty} \frac{1}{\alpha} j(\alpha e) = \begin{cases} \gamma\|e^D\|, & \text{if } \operatorname{tr} e = 0 \\ +\infty, & \text{if } \operatorname{tr} e \neq 0 \end{cases}, \quad \forall e \in \mathbb{R}^{3\times 3}_{sym}$$

and the corresponding problem of the limit analysis (10) becomes:

$$\zeta^* = \inf_{\substack{v\in\mathbb{V},\ div\, v=0 \\ L(v)=1}} \int_\Omega \gamma\|\varepsilon(v)\|\, dx. \tag{13}$$

This is a non-smooth optimization problem involving the divergence-free constraint. Further, it is known that $\lambda^* = \zeta^*$ (see [14]).

2.3 The Drucker–Prager Yield Criterion

The set B of the admissible stresses for the Drucker–Prager yield criterion reads as follows:

$$B = \left\{\tau \in \mathbb{R}^{3\times 3}_{sym} \mid \frac{a}{3}\operatorname{tr}\tau + \|\tau^D\| \le \gamma\right\}, \quad a, \gamma > 0. \tag{14}$$

B is an unbounded cone with the hydrostatic axis and the apex $\tau = \frac{\gamma}{\alpha}\iota$. For the shape of the yield surface in the Haigh-Westergaard coordinates we refer to [5]. Assume that $\mathbb{C}$ is the same as in (12) and denote

$$q_s(e) := Ka(\operatorname{tr} e) + 2G\|e^D\| - \gamma, \quad q_a(e) := Ka(\operatorname{tr} e) - Ka^2\|e^D\| - \gamma, \quad e \in \mathbb{R}^{3\times 3}_{sym}.$$

Notice that $q_s \ge q_a$. Then

$$\begin{aligned} j(e) &= \frac{K}{2}(\operatorname{tr} e)^2 + G\|e^D\|^2 - \frac{1}{2(Ka^2+2G)}\left\{\left[(q_s(e))^+\right]^2 + \frac{2G}{Ka^2}\left[(q_a(e))^+\right]^2\right\} \\ &= \begin{cases} \frac{K}{2}(\operatorname{tr} e)^2 + G\|e^D\|^2, & \text{if } q_s(e) \le 0, \\ -\frac{\gamma^2}{2Ka^2} + \frac{\gamma}{a}\operatorname{tr} e + \frac{G}{Ka^2(Ka^2+2G)}q_a(e)^2, & \text{if } q_s(e) \ge 0 \ge q_a(e), \\ -\frac{\gamma^2}{2Ka^2} + \frac{\gamma}{a}\operatorname{tr} e, & \text{if } q_a(e) \ge 0, \end{cases} \end{aligned}$$

where g^+ denotes the positive part of g. Another form of j can be found in [9] as well as the proof of the equality $\lambda^* = \zeta^*$ which holds for sufficiently small values of the parameter a and under appropriate assumptions. Further,

$$j_\infty(e) = \begin{cases} \frac{\gamma}{a}\operatorname{tr} e, & \text{if } \operatorname{tr} e \ge a\|e^D\| \\ +\infty, & \text{if } \operatorname{tr} e \le a\|e^D\| \end{cases}$$

and

$$\zeta^* = \inf_{\substack{v\in\mathbb{V},\ L(v)=1 \\ div\, v \ge a\|\varepsilon^D(v)\|}} \int_\Omega \frac{\gamma}{a}\operatorname{div} v\, dx, \qquad \operatorname{div} v = \operatorname{tr}\varepsilon(v).$$

Unlike the von Mises yield criterion, the problem of limit analysis leads to minimization of a linear functional but subject also to the inequality constraint.

3 Truncation Method

The von Mises and Drucker–Prager yield criteria lead to the unbounded sets B. The same holds also for the Tresca or Mohr-Coulomb yield criteria. For the Cam-Clay or capped Drucker–Prager criteria, the set B is bounded. On the other hand, models with bounded yield surfaces are usually accompanied by internal variables like hardening/softening or damage and so they are not perfectly plastic. The mentioned yield criteria and many others are presented, e.g., in [5].

The aim of this section is to emphasize that the limit analysis is much simpler for bounded than for unbounded B. Using this fact, it is quite natural to consider the truncation method for unbounded B. This section summarizes the results presented in [8].

3.1 Limit Analysis for Bounded B

Assume that B is *bounded*. Owing to this fact, one can derive the following additional results:

- From (6), it is readily seen that j_∞ is everywhere real-valued:

$$j_\infty(e) = \sup_{\tau\in B} \tau : e < +\infty \quad \forall e \in \mathbb{R}^{3\times 3}_{sym} \tag{15}$$

- The load assumption (1) yields $\zeta^* < +\infty$.
- From the definitions of j and j_∞, i.e., (2) and (6), we have:

$$j_\infty(e) - c \le j(e) \le j_\infty(e) \quad \forall e \in \mathbb{R}^{3\times 3}_{sym}, \quad c := \sup_{\tau\in B} \frac{1}{2}\mathbb{C}^{-1}\tau : \tau. \tag{16}$$

- It holds:

$$\lambda^* = \zeta^*, \qquad \inf_{v\in\mathbb{V}} J_{\lambda^*}(v) < +\infty. \tag{17}$$

- The following criterion for λ to be admissible or not holds:

$$\lambda > \lambda^* \iff \exists v \in \mathbb{V} : \ J_\lambda(v) < -c|\Omega|, \quad c := \sup_{\tau\in B} \frac{1}{2}\mathbb{C}^{-1}\tau : \tau. \tag{18}$$

  Notice that the constant c is usually a priori known. This criterion leads to a *guaranteed and easily computable upper bound* of λ^*. Indeed, one can easily

construct a minimization sequence $\{u_n\}$ of J_λ in $\mathbb{V}$ or in its subspace since J_λ is convex and differentiable. If $J_\lambda(u_n) < -c|\Omega|$ for some n then λ is an upper bound of λ^*. We use this criterion to verify numerical results in Sect. 6.

3.2 Truncation Method for Unbounded B

For unbounded B, the assertions (15)–(18) do not hold, in general. For this reason, we consider truncations of B using an appropriate system $\{B_k\}$, $\overline{\bigcup_{k>0} B_k} = B$ of bounded subsets of B. With any B_k, we associate the functions $j_k, j_{k,\infty}$ and the limit load parameters λ_k^*, ζ_k^* analogously to j, j_∞, and λ^*, ζ^* for unbounded B, respectively. From Lemma 1, (2), and (6), it follows that

$$\left.\begin{array}{l} j_k \le j, \quad j_{k,\infty} \le j_\infty, \\ \zeta_k^* = \lambda_k^* \le \lambda^* \le \zeta^*, \\ \lim\limits_{k\to+\infty} j_{k,\infty}(e) = j_\infty(e) \ \forall e \in \mathbb{R}^{3\times 3}_{sym}. \end{array}\right\} \tag{19}$$

Therefore, λ_k^* is a lower bound of λ^* for any $k > 0$. Knowledge of a reliable lower bound of λ^* is important since it presents a safety parameter. The truncation method can be also interpreted as a penalty approach in the problem of limit analysis making use of $(19)_3$. Sufficient conditions ensuring $\lambda_k^* \to \lambda^*$ as $k \to +\infty$ are presented in [8].

The truncated B for the von Mises yield criterion can be defined as follows:

$$B_k = \left\{ \tau \in \mathbb{R}^{3\times 3}_{sym} \mid \ \frac{1}{3}|tr\,\tau| \le k\gamma, \quad \|\tau^D\| \le \gamma \right\}, \quad k > 0. \tag{20}$$

The functions j_k and $j_{k,\infty}$ associated with such B_k are derived in [8] and the criterion (18) reads:

$$\lambda > \lambda^* \iff \exists v \in \mathbb{V}: \quad \int_\Omega j_k(\varepsilon(v))\,dx - \lambda L(v) < -\frac{\gamma^2}{2}\left(\frac{k^2}{K} + \frac{1}{2G}\right)|\Omega|. \tag{21}$$

A similar truncation can be also used for the Drucker–Prager yield criterion:

$$B_k = \left\{ \tau \in \mathbb{R}^{3\times 3}_{sym} \mid \ \frac{a}{3}\mathrm{tr}\,\tau \ge -k\gamma, \quad \frac{a}{3}\mathrm{tr}\,\tau + \|\tau^D\| \le \gamma \right\}, \quad k \ge 1. \tag{22}$$

The functions j_k and $j_{k,\infty}$ associated with this B_k are derived in [8] and the criterion (18) reads:

$$\lambda > \lambda^* \iff \exists v \in \mathbb{V}: \quad \int_\Omega j_k(\varepsilon(v))\,dx - \lambda L(v) < -\frac{\gamma^2}{2}\left(\frac{k^2}{Ka^2} + \frac{(1+k)^2}{2G}\right)|\Omega|. \tag{23}$$

4 Indirect Incremental Method

By enlarging λ up to its limit value λ^*, one can define the direct incremental method of the limit analysis. Notice that λ must be enlarged adaptively since λ^* is unknown. In [2, 12], another parameter $\alpha \to +\infty$ has been introduced together with an auxiliary minimization problem enabling an indirect control of the loading process for $\lambda \to \lambda^*$ in a discretized version of the problem. This technique has been extended in [7] for the continuous setting of the problem using the duality approach in terms of stresses. Now, we present a more straightforward derivation.

To this end, we use the sequence $\{j_\alpha\}$, $\alpha > 0$, of functions defined by (5) which pointwisely converges to j_∞ as follows from (6). Define the function $\bar{\psi} : \mathbb{R}_+ \to \mathbb{R}_+$ by the following penalization of the limit analysis problem:

$$(\mathscr{P})^\alpha \qquad \bar{\psi}(\alpha) := \inf_{\substack{v\in\mathbb{V}\\ L(v)=1}} \int_\Omega j_\alpha(\varepsilon(v))\,dx, \quad \alpha > 0. \tag{24}$$

Problem $(\mathscr{P})^\alpha$ is a smooth convex program with just one linear constraint. Numerically, it is not difficult to solve it, however, it is worth mentioning that minimizers need not belong to $\mathbb{V}$ similarly as for problem $(\mathscr{P})_\lambda$. Further, it holds:

$$\begin{aligned}
\bar{\psi}(\alpha) &\overset{(17,5)}{=} \frac{1}{\alpha} \inf_{\substack{v\in\mathbb{V}\\ L(v)=\alpha}} \int_\Omega j(\varepsilon(v))\,dx = \frac{1}{\alpha} \inf_{v\in\mathbb{V}} \sup_{\lambda\in\mathbb{R}} \left\{ \int_\Omega j(\varepsilon(v))\,dx - \lambda(L(v)-\alpha) \right\} \\
&= \frac{1}{\alpha} \sup_{\lambda\in\mathbb{R}} \inf_{v\in\mathbb{V}} \left\{ \int_\Omega j(\varepsilon(v))\,dx - \lambda(L(v)-\alpha) \right\} \\
&= \sup_{\lambda\in\mathbb{R}} \left[\frac{1}{\alpha} \inf_{v\in\mathbb{V}} \left\{ \int_\Omega j(\varepsilon(v))\,dx - \lambda L(v) \right\} + \lambda \right] \\
&= \sup_{\lambda\in\mathbb{R}_+} \left[\frac{1}{\alpha} \inf_{v\in\mathbb{V}} J_\lambda(v) + \lambda \right] = \sup_{\lambda\in\mathbb{R}_+} \left[\frac{1}{\alpha}\phi(\lambda) + \lambda \right] \quad \forall \alpha > 0,
\end{aligned} \tag{25}$$

where $\phi(\lambda) = \inf_{v\in\mathbb{V}} J_\lambda(v)$. The properties of ϕ has been derived in [7]. Under the assumption (1), it holds that ϕ is negative, strictly concave, decreasing and continuous in $(0, \lambda^*)$. Further, ϕ has at least quadratic decrease at infinity when $\lambda^* = +\infty$. Otherwise, $\phi(\lambda) = -\infty$ for any $\lambda > \lambda^*$. These properties of ϕ ensure that the function $\lambda \mapsto \frac{1}{\alpha}\phi(\lambda) + \lambda$ has a unique maximizer in $\mathbb{R}_+$ for any $\alpha > 0$. This enables us to introduce the function

$$\psi(\alpha) = \arg\max_{\lambda\in\mathbb{R}_+} \left[\frac{1}{\alpha}\phi(\lambda) + \lambda \right], \quad \alpha > 0. \tag{26}$$

From [7], we know:

(i) ψ is nondecreasing, continuous, $\lim_{\alpha\to 0_+}\psi(\alpha)=0$, and $\lim_{\alpha\to+\infty}\psi(\alpha)=\lambda^*$;
(ii) if there exists a minimizer $u_\alpha\in\mathbb{V}$ in problem $(\mathscr{P})^\alpha$ then αu_α solves $(\mathscr{P})_\lambda$ for

$$\lambda=\psi(\alpha)=\int_\Omega \Pi_B(\varepsilon(\alpha u_\alpha)):\varepsilon(u_\alpha)\,dx. \tag{27}$$

Moreover, the right hand side in (27) does not depend on the choice of u_α with the above mentioned properties;
(iii) conversely, if u_λ is a solution to $(\mathscr{P})_\lambda$ then $\frac{u_\lambda}{L(u_\lambda)}$ solves $(\mathscr{P})^\alpha$ for $\alpha=L(u_\lambda)$.

From (i), we see that knowledge of ψ enables us to introduce the indirect incremental method of limit analysis which corresponds to $\alpha\to+\infty$. Moreover, the values $\psi(\alpha)$ approximate λ^* from below. From (ii), we see that the values $\psi(\alpha)$ can be computed solving problem $(\mathscr{P})^\alpha$. Formula (27) is more convenient from the numerical point of view than (26). Due to (iii), one can interpret the parameter α as the complience or the work of external forces. Notice that the inverse mapping $\psi^{-1}:\lambda\mapsto\alpha$ need not be singlevalued unlike ψ.

Remark 2 Using (24) and (25) it is not difficult to show that the function $\bar\psi$ has the same properties as ψ, i.e. $\bar\psi$ is nondecreasing, continuous, $\lim_{\alpha\to 0_+}\bar\psi(\alpha)=0$, and $\lim_{\alpha\to+\infty}\bar\psi(\alpha)=\lambda^*$. Moreover, $\bar\psi(\alpha)=\frac{1}{\alpha}\phi(\psi(\alpha))+\psi(\alpha)<\psi(\alpha)\quad\forall\alpha>0$.

5 Finite Element Approximation

In this section, classical finite element approximations are considered for computing bounds of the limit load in the generalized Hencky plasticity. Let $\{\mathbb{V}_h\}$ be a system of finite element subspaces of $\mathbb{V}$ which is limit dense in $\mathbb{V}$. For the sake of simplicity, we will not consider influences of a domain approximation and numerical integration. Due to this simplification, most of the results from [7, 8] proven for the linear simplicial elements (P_1-elements) can be straightforwardly extended for higher-order elements. We summarize them.

The discrete forms of $(\mathscr{P})_\lambda$ and $(\mathscr{P})^\alpha$ read as follows:

$$(\mathscr{P}_h)_\lambda\qquad \inf_{v_h\in\mathbb{V}_h} J_\lambda(v_h),\quad J_\lambda(v_h)=\int_\Omega j(\varepsilon(v_h))\,dx-\lambda L(v_h),\quad \lambda>0,$$

$$(\mathscr{P}_h)^\alpha\qquad \bar\psi_h(\alpha)=\inf_{\substack{v_h\in\mathbb{V}_h\\ L(v_h)=1}}\int_\Omega j_\alpha(\varepsilon(v_h))\,dx,\quad j_\alpha(e)=\frac{1}{\alpha}j(\alpha e),\quad \alpha>0.$$

Unlike the continuous setting, one can find minimizers in $\mathbb{V}_h$ of these problems for any $\alpha>0$ and any $\lambda<\lambda_h^*$, where

$$\lambda_h^*=\sup\{\lambda\ge 0\mid \inf_{v_h\in\mathbb{V}_h} J_\lambda(v_h)>-\infty\} \tag{28}$$

is the discrete limit load parameter. Solutions to $(\mathscr{P}_h)_\lambda$ and $(\mathscr{P}_h)^\alpha$ are related each other as in Sect. 4. Therefore, the discrete counterpart ψ_h of ψ can be defined as follows:

$$\psi_h(\alpha) = \int_\Omega \Pi_B(\varepsilon(\alpha u_{h,\alpha})) : \varepsilon(u_{h,\alpha})\, dx = \arg\max_{\lambda\in\mathbb{R}_+} \left[\frac{1}{\alpha}\phi_h(\lambda) + \lambda\right], \quad \alpha > 0, \quad (29)$$

where $u_{h,\alpha} \in \mathbb{V}_h$ is a solution to $(\mathscr{P}_h)^\alpha$, $\phi_h(\lambda) = \inf_{v_h\in\mathbb{V}_h} J_\lambda(v_h)$, again using that the value $\psi_h(\alpha)$ is independent of the choice of the solution to $(\mathscr{P}_h)^\alpha$. The function ψ_h is continuous, nondecreasing, and $\psi_h(\alpha) \to \lambda_h^*$ as $\alpha \to +\infty$.

The discrete problem of limit analysis reads: determine ζ_h^* such that

$$\zeta_h^* = \inf_{\substack{v_h\in\mathbb{V}_h,\\ L(v_h)=1}} J_\infty(v_h), \quad J_\infty(v_h) = \int_\Omega j_\infty(\varepsilon(v_h))\, dx. \quad (30)$$

If there exists $v_h \in \mathbb{V}_h$, $L(v_h) = 1$, such that $J_\infty(v_h) < +\infty$ then problem (30) has a minimizer $u_{h,\infty}$ and any sequence $\{u_{h,\alpha}\}_\alpha$ of the solutions to $(\mathscr{P}_h)^\alpha$ is bounded in $\mathbb{V}_h$ for any $h > 0$. It is possible to show (see [8]) that any accumulation point of $\{u_{h,\alpha}\}_\alpha$ minimizes (30), and it holds that $\lambda_h^* = \zeta_h^*$. If such v_h does not exist, then $\lambda_h^* = \zeta_h^* = +\infty$.

From Lemma 1 we see that $\lambda_h^* \geq \lambda^*$. Further, it is known from [7] that if B is bounded then

$$\lambda_h^* \to \lambda^*, \quad h \to 0_+. \quad (31)$$

If B is unbounded, then (31) does not hold, in general. For unbounded B, one can apply the truncation technique from Sect. 3 to the discretized problems. Let $\{B_k\}$ be a system of bounded, closed and convex subsets of B. As in Sect. 3 we associate with any B_k the functions j_k, $J_{k,\lambda}$ and the limit values λ_k^*, ζ_k^*. The discrete limit load parameters associated with B_k and $\mathbb{V}_h$ are denoted as $\lambda_{k,h}^*$ and $\zeta_{k,h}^*$. Then $\lambda_{k,h}^* = \zeta_{k,h}^*$ and the following criterion holds:

$$\lambda > \lambda_{k,h}^* (\geq \lambda_k^*) \iff \exists v_h \in \mathbb{V}_h : \quad J_{k,\lambda}(v_h) < -c_k|\Omega|, \quad c_k = \frac{1}{2}\sup_{\tau\in B_k} \|\tau\|^2_{\mathbb{C}^{-1}}. \quad (32)$$

In [7], pointwise convergence $\psi_h \to \psi$ has been established for $\mathbb{V}_h$ constructed by P_1-elements. However, just this result cannot be straightforwardly extended to higher order elements as the ones mentioned above. Therefore, we sketch another proof based on the function $\bar{\psi}$ and its discretization.

Lemma 3 *It holds:*

$$\lim_{h\to 0_+} \bar{\psi}_h(\alpha) = \bar{\psi}(\alpha) \quad \forall \alpha > 0. \tag{33}$$

Proof For any $v \in \mathbb{V}$, $L(v) = 1$, there is a sequence $\{v_h\}$, $v_h \in \mathbb{V}_h$, $L(v_h) = 1$, such that $v_h \to v$ in $\mathbb{V}$. Hence,

$$\bar{\psi}_h(\alpha) \le \int_\Omega j_\alpha(\varepsilon(v_h))\,dx \to \int_\Omega j_\alpha(\varepsilon(v))\,dx \quad \forall \alpha > 0.$$

At the same time, from the definitions of $\bar{\psi}_h$ and $\bar{\psi}$ it follows that $\bar{\psi}_h(\alpha) \ge \bar{\psi}(\alpha)$ for any $\alpha > 0$. Therefore, (33) holds.

Theorem 1 *It holds:*

$$\lim_{h\to 0_+} \psi_h(\alpha) = \psi(\alpha) \quad \forall \alpha > 0. \tag{34}$$

Proof (Sketch). It is possible to show that the sequence $\{u_{h,\alpha}\}_h$ of solutions to $(\mathscr{P}_h)^\alpha$ is bounded in $\mathbb{V}$ for any $\alpha > 0$. Therefore, (29) implies boundedness of the sequence $\{\psi_h(\alpha)\}_h$ for any $\alpha > 0$. Then there exist: $\bar{\lambda} \in \mathbb{R}_+$ and a subsequence $\{\psi_{h'}(\alpha)\}$ such that $\psi_{h'}(\alpha) \to \bar{\lambda}$ as $h' \to 0_+$. From [7], it follows that $\phi_{h'}(\lambda) \to \phi(\lambda)$ for any $\lambda \in \mathbb{R}_+$. Using the continuity of ψ_h, we arrive at $\phi_{h'}(\psi_{h'}(\alpha)) \to \phi(\bar{\lambda})$ and

$$\bar{\psi}_{h'}(\alpha) = \frac{1}{\alpha}\phi_{h'}(\psi_{h'}(\alpha)) + \psi_{h'}(\alpha) \to \frac{1}{\alpha}\phi(\bar{\lambda}) + \bar{\lambda} \overset{(17,33)}{=} \bar{\psi}(\alpha) = \frac{1}{\alpha}\phi(\psi(\alpha)) + \psi(\alpha).$$

From the definition of $\psi(\alpha)$, it follows that $\bar{\lambda} = \psi(\alpha)$ proving (34).

Remark 3 Observe that the only one assumption on $\{\mathbb{V}_h\}$ is needed: namely that this system is limit dense in $\mathbb{V}$.

6 Computable Bounds of λ^* and Numerical Experiments

Since λ^* is a safety parameter, reliable computable bounds of this quantity are important. Unlike [2, 7, 8, 12], we now use the P_2-elements with a 7-point numerical integration formula instead of the P_1-elements in order to reduce strong dependence on the mesh density observed just for the P_1-elements and unbounded yield surfaces. We use similar benchmarks for the von Mises and Drucker–Prager yield surfaces as in [7, 8]. The computational experiments presented below were implemented in MatLab.

6.1 Computable Bounds of λ^* and Numerical Methods

Notation λ^*, λ_h^*, ψ, ψ_h, $(\mathscr{P}_h)^\alpha$ will be related to unbounded B while λ_k^*, $\lambda_{k,h}^*$, ψ_k, $\psi_{k,h}$, $(\mathscr{P}_{k,h})^\alpha$, and $(\mathscr{P}_{k,h})_\lambda$ will be associated with a bounded subset B_k of B. For unbounded B, two kinds of lower bounds were mentioned: $\psi(\alpha), \alpha > 0$, and $\lambda_k^*, k > 0$. Convergence $\psi_h(\alpha) \to \psi(\alpha)$ and $\lambda_{k,h}^* \to \lambda_k^*$ as $h \to 0_+$ hold for the bounds but $\lambda_h^* \to \lambda^*$ need not hold, in general. Values $\lambda_{k,h}^*$ can be approximated from below by $\psi_{k,h}(\alpha)$ where α is sufficiently large. Moreover, the guaranteed upper bound (32) of $\lambda_{k,h}^*$ and λ_k^* is at our disposition. This bound should be close to $\psi_{k,h}(\alpha)$ for verification of numerical results. Further, λ^* will be estimated from above by $\lambda_h^* \approx \psi_h(\alpha)$, where α is sufficiently large. We will compare numerically the mentioned bounds for several meshes.

The functions ψ_h and $\psi_{k,h}$ can be assessed solving $(\mathscr{P}_h)^\alpha$ and $(\mathscr{P}_{k,h})^\alpha$, respectively. To this end, we use the semismooth Newton method with damping or as a case may be with regularized tangent stiffness matrices. In the latter case the tangent stiffness matrix is replaced by a convex combination of the tangent and elastic stiffness matrices to get positive definiteness. Damped parameters belong to $(0, 1]$ and guarantee a decrease of minimized functions in the Newton direction. In context of the minimization problem, the method can be interpreted as a sequential quadratic programming approach. The load constraint is enforced by the Lagrange multiplier in each Newton's iteration. For convergence analysis and numerical experiments with the variants of the semismooth Newton method we refer to [2]. We use the relative tolerance $1e-10$ in a termination criterion of the Newton-like method.

This enables us to construct the loading $\lambda - \alpha$ curve to estimate λ_h^*. Firstly, a constant increment $\delta\alpha > 0$ is considered. If the computed increment $\delta\lambda$ is less than the prescribed threshold (we use 0.001) then we enlarge $\delta\alpha$ twice. So the values of α can growth exponentially in a vicinity of the limit load. The loading process is terminated when either $\alpha > \alpha_{max}$ or $\delta\lambda \ll 0.001$.

Denote $\bar{\alpha}_h$ as the maximal value of α obtained in this way for given $\mathscr{T}_h$ and B. For the truncation B_k, we write $\bar{\alpha}_{k,h}$ to emphasize also dependence on k. We use the values $\psi_h(\bar{\alpha}_h)$ and $\bar{\lambda}_{k,h} = \psi_{k,h}(\bar{\alpha}_{k,h})$ as an approximation of λ_h^* and as a lower bound of $\lambda_{k,h}^*$, respectively. In order to find the guaranteed upper bound of $\lambda_{k,h}^*$, we contruct a minimization sequence of problem $(\mathscr{P}_{h,k})_\lambda$ using the damped semismooth Newton method. We observed that the value $\lambda = \bar{\lambda}_{k,h} + \delta\lambda$, where $\delta\lambda = 0.001$, is usually sufficient to satisfy criterion (32). Otherwise, we enlarge $\delta\lambda$.

6.2 Numerical Example with the Von Mises Criterion

We consider a benchmark used in [7, 8] and many other papers, namely a plane strain problem with Ω depicted in Fig. 1: Ω is a quarter of the 10×10 (m) square with the circular hole of radius 1 (m) in its center. The constant traction of density $f = (0, 450), (0, 0)$ (MPa) acts on the upper, and the right vertical side, respec-

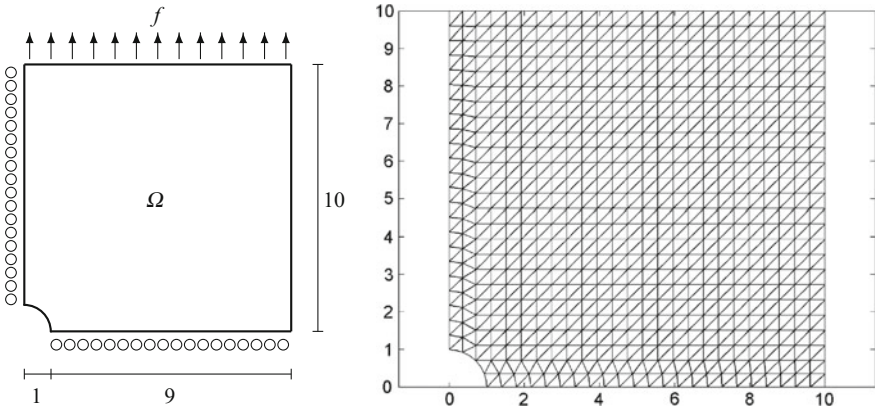

Fig. 1 Geometry and triangulation

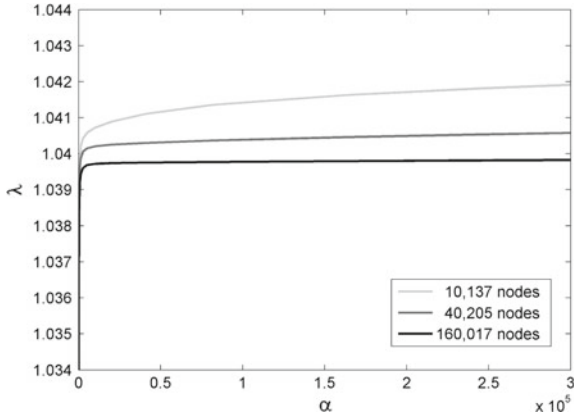

Fig. 2 Loading paths (zoom) for B

tively. The volume forces are neglected. This load corresponds to $\lambda = 1$. On the rest of $\partial\Omega$ the symmetry boundary conditions are prescribed. The material parameters are set as follows: $E = 206900$ MPa (Young's modulus), $\nu = 0.29$ (Poisson's ratio) and $\gamma = 450\sqrt{2/3}$ MPa. Hence, the values of K and G needed in (12) are $K = \frac{E}{3(1-2\nu)}$ and $G = \frac{E}{2(1+\nu)}$. To obtain more accurate bounds than in [7, 8], we use the P_2-elements, a different mesh structure depicted in Fig. 1, and the truncation coefficient $k = 0.7$ for defining B_k.

The loading paths represented by the graphs of ψ_h and $\psi_{k,h}$ are computed and compared for three different triangulations $\mathcal{T}_h$ with 10,137, 40,205, and 160,017 nodes (including the midpoints). Notice that the mesh in Fig. 1 has 2,585 nodes. Zoom of the resulting loading paths in a vicinity of the limit load is depicted in Fig. 2 for B and in Fig. 3 for B_k.

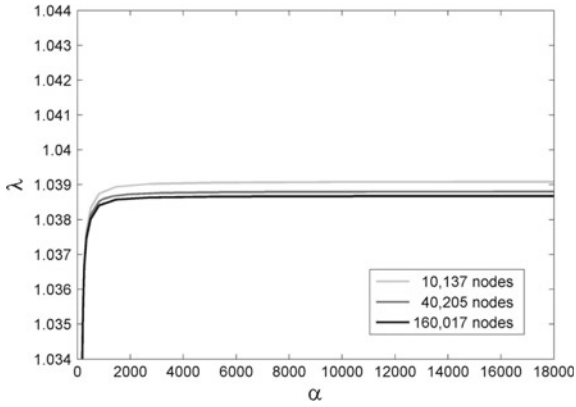

Fig. 3 Loading paths (zoom) for B_k, $k = 0.7$

Table 1 Lower and upper bounds of $\lambda^*_{k,h}$, $k = 0.7$

No. of nodes	10,137	40,205	160,017
Lower bound	1.0391	1.0388	1.0387
Upper bound	1.0401	1.0398	1.0397

One can observe that for any $\alpha > 0$ fixed, the sequences $\{\psi_h(\alpha)\}_h$ and $\{\psi_{k,h}(\alpha)\}_h$ are decreasing and converging. Moreover, the curves are almost constant for sufficiently large values of α. In Fig. 2, this is visible only for the finest mesh (black color) due to the zoom. From the black curve, we obtain the value close to 1.040 as a reliable upper bound of λ^*. The curves for B_k are less dependent on the number of nodes of $\mathscr{T}_h$ than for B. The computed values $\psi_{k,h}(\bar{\alpha}_{k,h})$, i.e., the lower bounds of $\lambda^*_{k,h}$ are shown in Table 1 and compared with the guaranteed upper bounds of $\lambda^*_{k,h}$. The bounds practically coincide for the used meshes. This confirms that our results are reliable. From Table 1 we see that $\lambda^*_k \approx 1.038$.

We arrive at the following bounds of λ^*: $1.038 \leq \lambda^* \leq 1.040$. Further, it is useful to have a look at Figs. 4 and 5 where the displacements in the horizontal and vertical directions (solution to $(\mathscr{P}_h)^\alpha$) at the end of the loading process (i.e. $\alpha = \bar{\alpha}_h$) are depicted for B and the finest mesh.

We observe a significant jump of the values along the same thin diagonal band. Far from it, the material is rigid (constant displacements) which is in accordance with Remark 1. Moreover, the vector field depicted in these figures can be simply approximated by the function $v_\delta = (v_{\delta,1}, v_{\delta,2})$, where $\delta > 0, \delta << 1$,

$$v_{\delta,1}(x,y) = \begin{cases} 0, & \text{if } y - x + 1 \geq \delta \\ \frac{a}{\delta}(y - x + 1 - \delta), & \text{if } 0 \leq y - x + 1 \leq \delta \\ -a, & \text{if } 0 \geq y - x + 1 \end{cases},$$

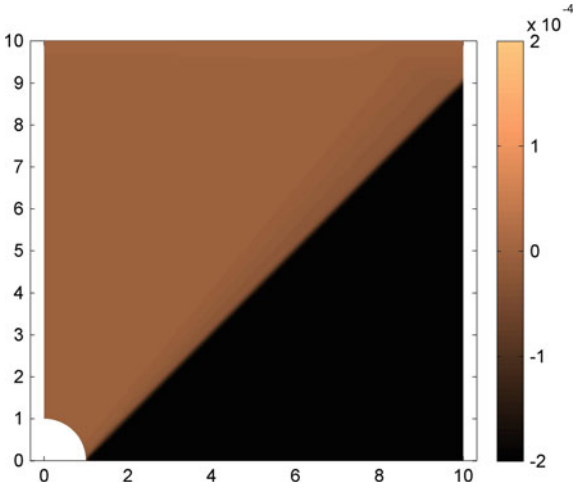

Fig. 4 Horizontal displacements for B

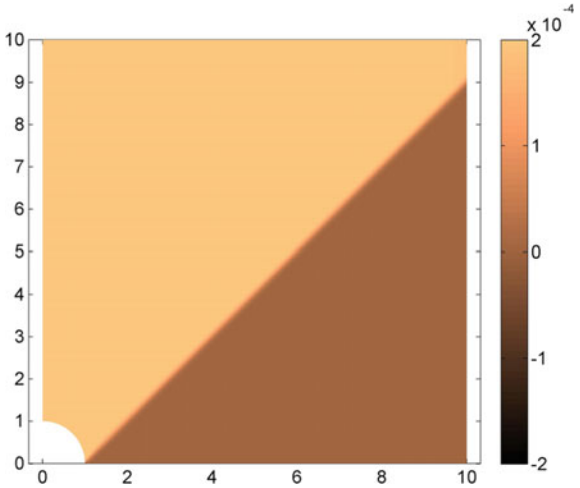

Fig. 5 Vertical displacements for B

$$v_{\delta,2}(x,y) = \begin{cases} a, & \text{if } y - x + 1 \geq \delta \\ \frac{a}{\delta}(y - x + 1), & \text{if } 0 \leq y - x + 1 \leq \delta \\ 0, & \text{if } 0 \geq y - x + 1 \end{cases}, \quad a = \frac{1}{4500}.$$

It is easy to see that $v_\delta \in \mathbb{V}$, $\operatorname{div} v_\delta = 0$ in Ω, and $L(v_\delta) = 1$ for any $\delta \ll 1$. Therefore, from (13), we have:

$$\lambda^* \leq \int_\Omega \gamma \, \|\varepsilon(v_\delta)\| \, dx = \gamma \frac{a}{\delta} \sqrt{2} |\Omega_\delta| = \frac{9}{5\sqrt{3}} + O(\delta) \doteq 1.0392 + O(\delta),$$

where $\Omega_\delta = \{(x, y) \in \Omega \mid 0 \le y - x + 1 \le \delta\}$ and $|\Omega_\delta| = 9\delta + O(\delta^2)$. Hence, the value 1.0392 is a guaranteed upper bound of λ^* which is fully in accordance with our numerical results. Notice that the sequence $\{v_\delta\}$ is converging to a function which belongs to $BD(\Omega; \mathbb{R}^2) \setminus \mathbb{V}$.

In [7, 8], a much more pessimistic upper bound was obtained for the P_1-elements. Moreover, the corresponding curves for B strongly depended on the mesh. On the other hand, for B_k, the results for P_1 and P_2-elements are similar. So, it seems that the truncation limit analysis is useful for P_2-elements and necessary for P_1- elements.

6.3 Numerical Example with the Drucker–Prager Criterion

The second example is a slope stability benchmark considered as a plane strain problem [3, 5, 13]. In comparison to [5, 8, 13], we use much smaller geometry and the Poisson ratio $\nu = 0.25$ instead of $\nu = 0.49$. From Remark 1, it follows that the limit load parameter should be independent of these settings. The shape and sizes of 2D domain Ω with a uniform triangular mesh are shown in Fig. 6. The slope inclination is 45°. On the bottom we assume that Ω is fixed and the zero normal displacements are prescribed on both vertical sides. The remaining part of $\partial\Omega$ is free. The load L is represented by the gravity force F. We set the specific weight $\rho g = 20\,\mathrm{kN/m^3}$ with ρ being the mass density and g the gravitational acceleration. The Drucker- Prager parameters a and γ appearing in (14) are computed from the friction angle ϕ and the cohesion c as follows [5]:

$$a = \frac{3\sqrt{2}\tan\phi}{\sqrt{9 + 12(\tan\phi)^2}}, \quad \gamma = \frac{3\sqrt{2}c}{\sqrt{9 + 12(\tan\phi)^2}}.$$

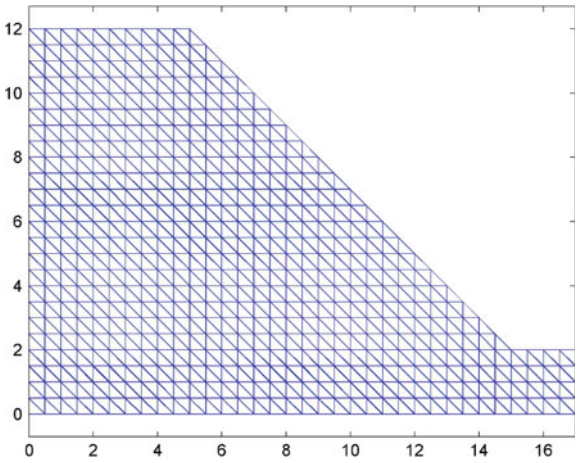

Fig. 6 Geometry of the problem and the mesh for $h = 0.5\,\mathrm{m}$

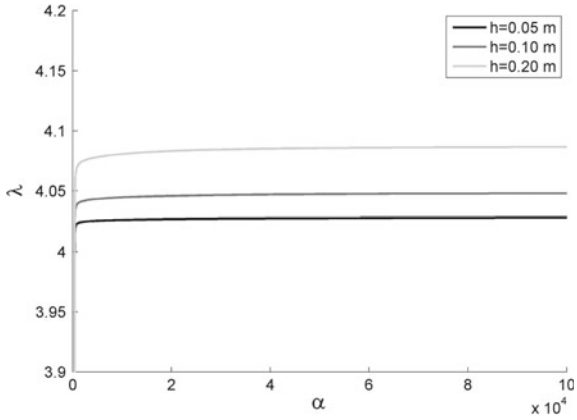

Fig. 7 Loading paths for B

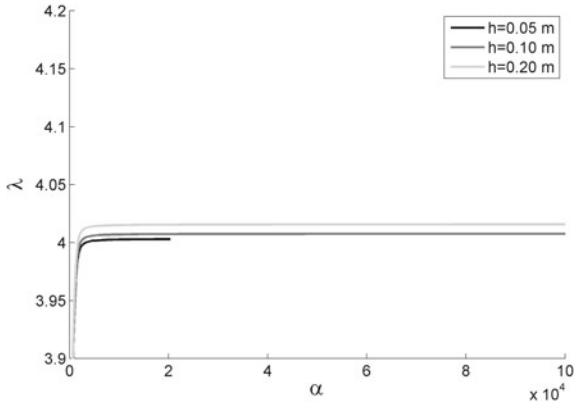

Fig. 8 Loading paths for B_k, $k = 3.9$

Finally, $E = 20\,000$ kPa, $\phi = 20°$ and $c = 50$ kPa. The bulk and shear moduli are computed as in Sect. 6.2. The discretization of $(\mathscr{P}_h)^\alpha$ is done by P_2-elements using three uniform triangulations $\mathscr{T}_h$ of $\bar{\Omega}$ with $h = 0.05,\ 0.1,\ 0.2$ meters, where h stands for the length of the leg of the isosceles right triangles creating $\mathscr{T}_h$.

The loading paths for all these meshes are depicted in Figs. 7 and 8 for $\alpha \in [0, 1e5]$. In Fig. 7 we see the loading paths for the original set B defined by (14). Again, one can observe that the curves converge to some limit curve. Since the paths are almost constant for $\alpha > 2e4$ the respective values of ψ_h at $\alpha = 1e5$ can be considered to be equal to λ_h^*. Consequently, $\lambda^*_{h=0.05} = 4.03$ is a reliable upper bound of λ^*.

To get a lower bound of λ^* we use the truncation approach with B_k defined by (22). Figure 8 depicts the resulting loading paths for $B_{k=3.9}$. The curves are less dependent on the number of the nodes of $\mathscr{T}_h$ than for B. The computed values $\psi_{k,h}(\bar{\alpha}_{k,h})$, i.e., the lower bounds of $\lambda^*_{k,h}$ are displayed in Table 2 and compared with the guaranteed upper bounds of $\lambda^*_{k,h}$. The bounds practically coincide for the used meshes. This confirms the reliability of our results. From Table 2, we see that $\lambda^*_k \approx 4.00$.

Table 2 Lower and upper bounds of $\lambda^*_{k,h}$, $k = 3.9$

No. of nodes	$h = 0.20$	$h = 0.10$	$h = 0.05$
Lower bound	4.016	4.008	4.003
Upper bound	4.017	4.009	4.005

Based on this experiment we may conclude that the values 4.00 and 4.03 could serve as reliable lower and upper bounds to λ^*, respectively. The analytical estimate to this problem for the Mohr-Coulomb yield function presented in [3] gives the value $\lambda^* \approx 4.045$ which is close to the computed bounds.

7 Conclusion

The paper completes our research presented in [2, 7, 8, 12]. Unlike these papers, some results are extended to P_2-elements. For quadratic elements and unbounded yield surfaces, the loading paths are not so much dependent on the number of mesh nodes as for P_1-elements. On the other hand, for bounded yield surfaces, P_1 and P_2-elements, we obtain more or less the same results. We also illustrated using the slope stability benchmark that the limit load parameter is independent of the elastic parameters and the size of the geometry. These facts enable us to significantly improve estimates of λ^* in comparison to [7, 8].

Acknowledgements This work was supported by The Ministry of Education, Youth and Sports of the Czech Republic from the National Programme of Sustainability (NPU II), project "IT4 Innovations excellence in science - LQ1602".

References

1. Caboussat, A., Glowinski, R.: Numerical solution of a variational problem arising in stress analysis: the vector case. Discret. Contin. Dyn. Syst. **27**, 1447–1472 (2010)
2. Cermak, M., Haslinger, J., Kozubek, T., Sysala, S.: Discretization and numerical realization of contact problems for elastic-perfectly plastic bodies. PART II – numerical realization. ZAMM-Journal of Applied Mathematics and Mechanics/Zeitschrift für Angewandte Mathematik und Mechanik **95**, 1348–1371 (2015)
3. Chen, W., Liu, X.L.: Limit analysis in soil mechanics. Elsevier, Amsterdam (1990)
4. Christiansen, E.: Limit analysis of colapse states. In: Ciarlet, P.G., Lions, J.L.: (eds.) Handbook of Numerical Analysis, vol. IV, Part 2, pp. 195–312. North-Holland (1996)
5. de Souza Neto, E.A., Perić, D., Owen, D.R.J.: Computational Methods for Plasticity: Theory and Application. Wiley, New Jersey (2008)
6. Duvaut, G., Lions, J.L.: Inequalities in Mechanics and Physics. Springer, Berlin (1976)
7. Haslinger, J., Repin, S., Sysala, S.: A reliable incremental method of computing the limit load in deformation plasticity based on compliance: Continuous and discrete setting. J. Comput. Appl. Math. **303**, 156–170 (2016)
8. Haslinger, J., Repin, S., Sysala, S.: Guaranteed and computable bounds of the limit load for variational problems with linear growth energy functionals. Appl. Math. **61**, 527–564 (2016)

9. Repin, S., Seregin, G.: Existence of a weak solution of the minimax problem arising in Coulomb-Mohr plasticity. In: Nonlinear Evolution Equations, American Mathematical Society Translations: (2), vol. 164, pp. 189–220. American Mathematical Society, Providence, RI (1995)
10. Suquet, P.: *Existence et régularité des solutions des équations de la plasticité parfaite*, These de 3e Cycle, Université de Paris VI (1978)
11. Sysala, S.: Properties and simplifications of constitutive time-distretized elastoplastic operators. ZAMM-Journal of Applied Mathematics and Mechanics/Zeitschrift für Angewandte Mathematik und Mechanik **94**, 233–255 (2014)
12. Sysala, S., Haslinger, J., Hlaváček, I., Cermak, M.: *Discretization and numerical realization of contact problems for elastic-perfectly plastic bodies. PART I – discretization, limit analysis*. ZAMM-Journal of Applied Mathematics and Mechanics/Zeitschrift für Angewandte Mathematik und Mechanik **95**, 333–353 (2015)
13. Sysala, S., Cermak, M., Koudelka, T., Kruis, J., Zeman, J., Blaheta, R.: *Subdifferential-based implicit return-mapping operators in computational plasticity*. ZAMM-Journal of Applied Mathematics and Mechanics/Zeitschrift für Angewandte Mathematik und Mechanik **96**, 1318–1338 (2016)
14. Temam, R.: Mathematical Problems in Plasticity. Gauthier-Villars, Paris (1985)